CRREL REPORT 91-3

Computer Model of Atmospheric Ice Accretion on Transmission Lines

Kathleen F. Jones and Kurt Z. Egelhofer

February 1991

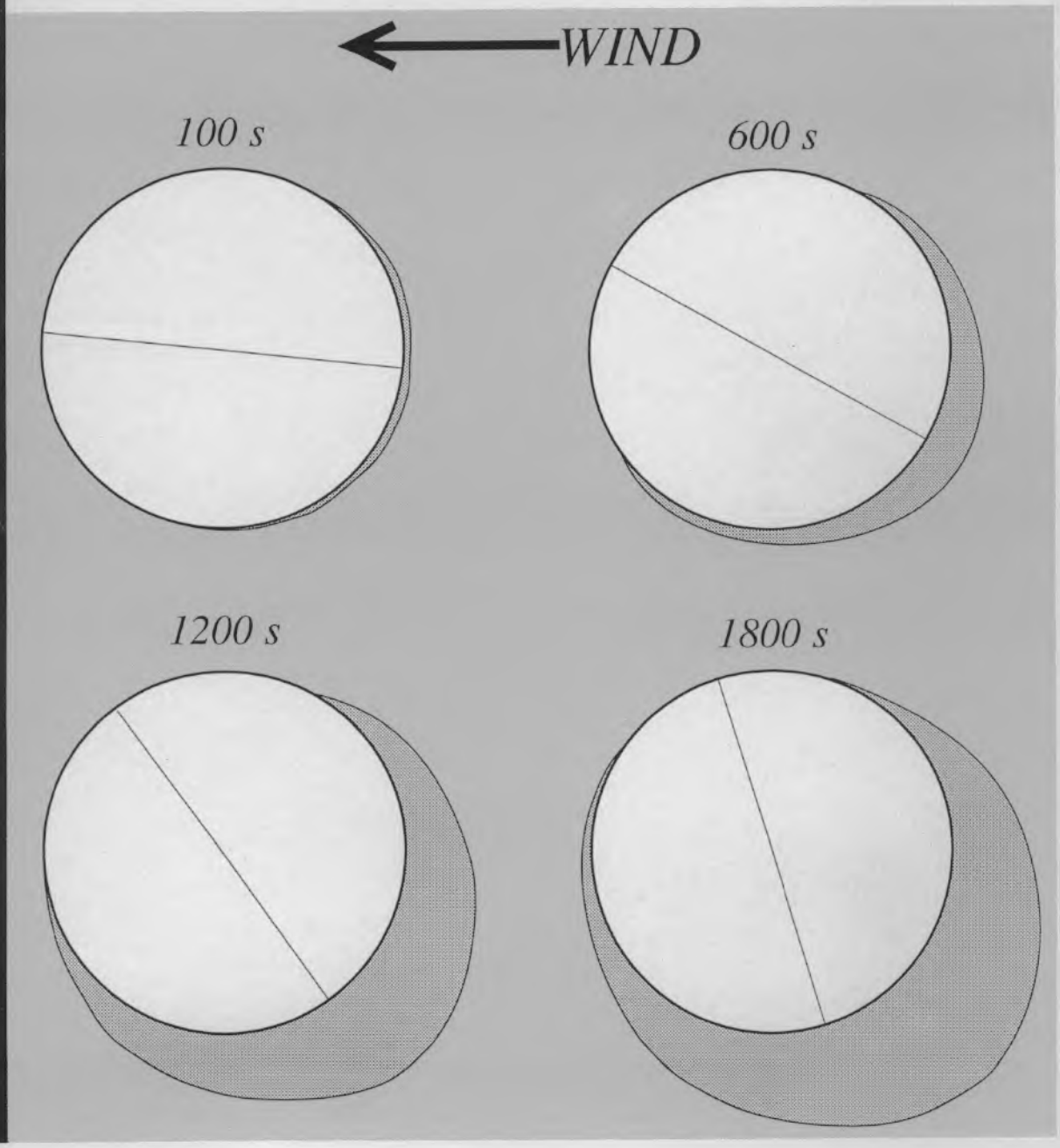

For conversion of SI metric units to U.S./British customary units of measurement consult ASTM Standard E380, Metric Practice Guide, *published by the American Society for Testing and Materials, 1916 Race St., Philadelphia, Pa. 19103.*

Cover: Cross section of a transmission line with a growing ice accretion, showing how the wire rotates as the accretion gets larger.

CRREL Report 91-3

U.S. Army Corps of Engineers
Cold Regions Research & Engineering Laboratory

Computer Model of Atmospheric Ice Accretion on Transmission Lines

Kathleen F. Jones and Kurt Z. Egelhofer

February 1991

Prepared for
OFFICE OF THE CHIEF OF ENGINEERS

PREFACE

This report was prepared by Kathleen F. Jones, Research Physical Scientist, Snow and Ice Branch, Research Division, U.S. Army Cold Regions Research and Engineering Laboratory, and Kurt Z. Egelhofer, graduate student, Thayer School of Engineering, Dartmouth College. Funding for this research was provided by DA Project 4A161102AT24, Work Unit FS/005, *Concepts for Spatial Winter Boundary Layer Description.* The authors thank Jacqueline Richter-Menge and Kazuhiko Itagaki for reviewing the report.

CONTENTS

ILLUSTRATIONS

Figure

TABLE

Table

NOMENCLATURE

A surface area of heat transfer per meter of wire (m)
C_d drag coefficient
C_l lift coefficient
C_{pa} heat capacity of air (J/kg °C)
C_{pc} heat capacity per unit length of wire and ice accretion (J/m °C)
C_{pi} heat capacity of ice (J/kg °C)
C_{pw} heat capacity of water (J/kg °C)
d distance from center of wire to ice center of mass (m)
d_x horizontal distance from center of wire to ice center of mass (m)
d_y vertical distance from center of wire to ice center of mass (m)
D diameter of wire or cylinder (m)
D_i diameter of wire and ice accretion normal to the flow (m)
E global collection efficiency
E_o saturation vapor pressure of water over ice at T_o (N/m^2)
E_s vapor pressure of water over ice at T_s (N/m^2)
F_a fraction of water accreted as ice
F_i force due to weight of ice (N)
F_l lift force (N)
F_x horizontal force (N)
F_y vertical force (N)
g gravitational acceleration (m/s^2)
G shear modulus (N/m^2)
h convective heat transfer coefficient (W/m^2 °C)
h_i ice accretion thickness (m)
J polar moment of inertia (m^4)
k dimensionless inertia parameter
k_a molecular thermal conductivity of air (W/m °C)
K wire torsional stiffness (Nm/radian)
$\bar{l}$ wire–ice surface vector at droplet impact point
L dimensionless distance along airfoil surface from stagnation point
L_w total length of wire (m)
L_f latent heat of fusion of water (J/kg)
L_v latent heat of vaporization of water (J/kg)
$\dot{m}$ ice accretion mass flux (kg/m^2s)
m_i mass of ice accretion (kg)
P atmospheric pressure (N/m^2)
Q change in heat content per meter of wire (J/m)
r droplet radius (m)
R $-10^6 r V_o/T_s$
Re droplet Reynolds number

R_s surface recovery factor

t time (s)

$\bar{t}$ dimensionless time

Δt time increment (s)

T torque (Nm)

T_f film temperature (°C)

T_o ambient air temperature (°C)

T_s wire–ice surface temperature (°C)

U flow velocity (m/s)

$\bar{U}$ dimensionless flow velocity

U_o uniform far-field flow velocity (m/s)

u_x x component of flow velocity (m/s)

u_y y component of flow velocity (m/s)

V droplet velocity (m/s)

$\bar{V}$ dimensionless droplet velocity

V_o droplet impact speed at stagnation line (m/s)

W liquid water content (kg/m^3)

x horizontal coordinate

y vertical coordinate

Y dimensionless ordinate of droplet trajectory starting point

z distance along wire (m)

α airfoil angle of attack (radians)

β local collection efficiency

γ cylinder angle, measured from stagnation line (degrees)

δ incremental rotation of wire (radians)

ψ stream function (m^2/s)

ϕ velocity potential (m^2/s)

μ dynamic viscosity of air (kg/m s)

ν kinematic viscosity of air (m^2/s)

ρ_a density of air (kg/m^3)

ρ_i density of ice (kg/m^3)

ρ_w density of water (kg/m^3)

θ rotation of wire (radians)

$\bar{\theta}$ average rotation of wire fixed at both ends (radians)

Computer Model of Atmospheric Ice Accretion on Transmission Lines

KATHLEEN F. JONES AND KURT Z. EGELHOFER

INTRODUCTION

Atmospheric icing occurs in conditions where the cooling of an air mass causes the supercooling of water droplets. Water droplets in the atmosphere can remain in the liquid state at air temperatures as low as –40°C before spontaneous freezing occurs (Battan 1962). Aircraft operating in these supercooled clouds experience structural icing as the water droplets hit the aircraft and freeze. Icing can occur at the earth's surface in a supercooled fog or during freezing rains. Under these conditions ice will accrete on structures with surface temperatures below freezing.

Ice accretion problems are of interest to engineers and scientists because ice growth on manmade structures can lead to structural failure and the subsequent loss of human life or property. Widely known examples of failure due to ice growth include aircraft crashes, tower collapses and transmission line failures leading to power outages. Researchers have approached the accretion problem with three techniques: computer modeling studies, laboratory studies and field studies. Recent attempts at modeling transmission line icing have resulted in the quantification of many of the important aspects of the problem, including liquid water droplet interactions with the air flow, the variation of local collection efficiency of the accreting object, thermodynamic processes at the freezing surface, the torsional response of flexible structures to asymmetric loads, and aerodynamic forces on the structure.

Research on the accretion of atmospheric ice on ground-based structures has taken a variety of directions: estimating the probability of an icing event, estimating the expected hazards of an event, and devising strategies to mitigate or eliminate ice accretions. Many potential problems can be avoided through prudent planning in conjunction with climatological and meteorological studies. For example, Mallory and Leavengood (1983) described the successful relocation of a Southern California Edison Company 500-kV transmission line based on meteorological studies that predicted frequent icing events along a segment of the original route. However, atmospheric icing is a fairly widespread phenomenon, and the expansion of activities into mountainous and subarctic regions has forced engineers and scientists to address the problem directly. The lack of historical meteorological data in remote locations has hindered attempts to determine icing parameters and to predict the occurrence and severity of icing storms. For these reasons recent research has concentrated on understanding the physical accretion process and developing models to predict the severity of icing events (for example, Ackley and Templeton 1979, Lozowski and Oleskiw 1983, McComber et al. 1983, Smith and Barker 1983). Model results have been verified by comparison with field and laboratory data. Additionally, field measurements of icing conditions have become more frequent in recent years (for example, McComber et al. 1982, Govoni and Ackley 1983, Krishnasamy 1983, Tattleman 1983). However, a literature review quickly reveals how sparse the data base is, making it difficult to use existing data for a specific application or geographical area.

This study focuses on modeling the formation of ice accretions on flexible structures such as transmission lines. The model requires the input of meteorological and icing parameters and predicts the vertical and horizontal loads on the support structures of the transmission line for a given structural design. The design engineer can then decide to adjust the structural design or the transmission line location or both to mitigate ice accretion loads.

ATMOSPHERIC ICING PROCESS

Ice accretions have been classified according to source and outward appearance (Makkonen 1984a). Glaze and rime ice, which occur in many severe icing events, form from supercooled water droplets. Glaze is a hard, nearly bubble-free and clear homogeneous ice with a density close to 0.92 Mg/m^3, the density of pure bubble-free ice. Glaze ice grows "wet," and water may run back along the structure. Rime ice, on the other hand, grows "dry," that is, water droplets impinging on the structure freeze on impact. Hard rime is a rather hard, granular, white or translucent ice with a density between 0.6 and 0.9 Mg/m^3. Soft rime is white ice with a loose structure and a density less than 0.6 Mg/m^3. There are two other types of ice accretions: hoarfrost, which grows directly from water vapor, and wet snow, which originates from snowflakes. Because many severe icing events involve glaze and rime ice, this study focused on these types of icing.

Rime and glaze ice are formed when supercooled water droplets impinge on a structure and adhere to the surface by freezing. Ackley and Templeton (1979) identified six variables necessary to quantify the amount and character of accreted ice on a structure: ambient air temperature, cloud liquid water content and droplet size distribution, wind speed, and cross-sectional diameter and shape of the object. Both the liquid water content and the droplet size distribution are difficult to measure. Unfortunately the amount of ice that will accrete on a wire is extremely sensitive to droplet size, as shown in Figure 1 (Makkonen 1984b). The air temperature and wind speed are more easily measured, but as mentioned previously, an extensive data base for remote locations does not exist. The shape of an iced object may be complex and may change as the ice accretion grows and the effective size of the structure changes.

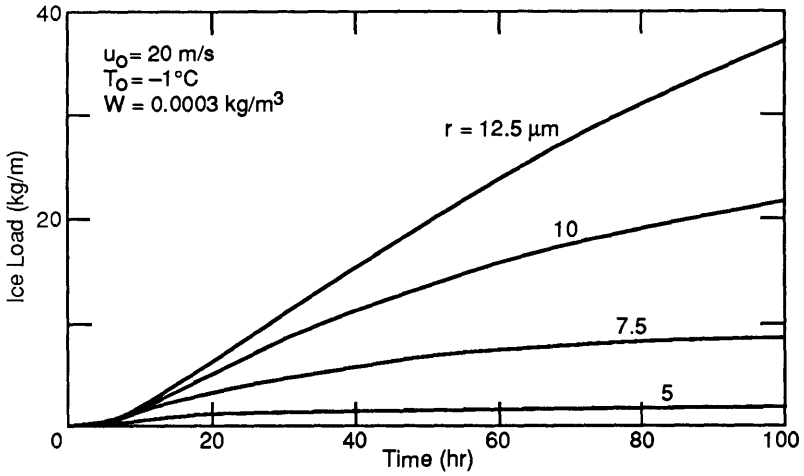

Figure 1. Dependence of accreted ice load on the median volume droplet diameter. (After Makkonen 1984b.)

When a transmission line is exposed to icing conditions, the rate of ice accretion is governed by two processes that depend on the above variables: the impingement of supercooled water droplets on the wire, and the thermodynamics at the wire surface, which determines what portion of the impinging water freezes or, on the other hand, melts previously accreted ice. Each of these processes will be discussed from the standpoint of how previous researchers have approached the problem.

DROPLET TRAJECTORIES

For flow velocities at which atmospheric icing occurs, the air flow around a long uniform object

can be treated as two-dimensional, steady, incompressible, irrotational fluid flow. Therefore, potential theory can be used to describe the velocity field, and the flow satisfies Laplace's equation in the entire plane (Batchelor 1970):

$$\partial^2\phi/\partial x^2 + \partial^2\phi/\partial y^2 = 0 \qquad \partial^2\psi/\partial x^2 + \partial^2\psi/\partial y^2 = 0 \tag{1}$$

where x = horizontal coordinate
y = vertical coordinate
ϕ = velocity potential
ψ = stream function.

Lines of constant ψ are the streamlines of the flow, which are perpendicular to the lines of constant ϕ. The air velocity components can be determined at any point in the air stream by differentiating the stream function:

$$u_x = \partial\psi/\partial y \qquad u_y = -\partial\psi/\partial x \tag{2}$$

where u_x is the x component of the flow velocity and u_y is the y component of the flow velocity. The stream function and velocity potential are related through the Cauchy–Riemann equations of complex variable theory:

$$\partial\psi/\partial y = \partial\phi/\partial x \qquad \partial\psi/\partial x = -\partial\phi/\partial y. \tag{3}$$

For cylinders with circular or elliptical cross sections, the velocity at any point in the airstream can be determined analytically (Ackley and Templeton 1979). For arbitrary cross-sectional shapes, such as airfoils or iced transmission lines that are free to rotate, transformation or numerical techniques must be employed. These techniques can be broadly classified into three groups:

- Conformal transformation techniques (Theodorson and Garrick 1932);
- Surface singularity methods (Hess and Smith 1967); and
- Finite-element techniques (McComber and Touzot 1981).

Lozowski and Oleskiw (1983) emphasized that the technique chosen should be efficient in terms of computer time because of the large number of velocity calculations necessary to compute the water droplet trajectories, and it should be capable of adjusting to a changing object cross section as ice accretes.

To determine the kinematic interaction between the water droplets in the air stream and a transmission line, the equation of motion for the droplets must be solved. Ackley and Templeton (1979) based their analytic approach for a cylinder with an elliptical cross section on the work of Brun (1957). The assumptions for this formulation are:

- The concentration of droplets in the air stream is sufficiently small that the flow is not perturbed by the droplets;
- The force of gravity is much less than the inertial forces and can be neglected; and
- The pressure forces on a droplet are equal to those on an equivalent volume of air at the same location, and these forces can be neglected because the density of water is much greater than that of air.

The motion of the droplet therefore depends primarily on its inertia and the viscous drag force on the droplet due to the deflection of the air stream around the cylinder.

Langmuir and Blodgett (1946) formulated this problem for a cylinder and solved Newton's second law of motion in dimensionless form:

$$k\, d\bar{V}/d\bar{t} = -C_d Re\left(\bar{V}-\bar{U}\right)/24 \tag{4}$$

where C_d = drag coefficient
$\bar{V}$ = V/U_o
$\bar{U}$ = U/U_o
$\bar{t}$ = $2tU_o/D$
Re = $2\rho_a r|V-U|/\mu$ (droplet Reynolds number)
k = $4\rho_w r^2 U_o/(9\mu D)$ (inertia parameter)
U_o = uniform far-field flow velocity
U = flow velocity
V = droplet velocity
t = time
ρ_w = density of water
ρ_a = density of air
μ = dynamic viscosity of air
r = droplet radius
D = cylinder diameter.

The functional dependence of the drag coefficient of a spherical droplet in an air stream on the Reynolds number has been determined experimentally by several researchers. Beard and Pruppacher (1969) reported the following formulas for C_d:

$$\begin{aligned} C_d &= 24\,(1+0.102\,Re^{0.955})/Re && \text{for } 0.2 < Re < 2 \\ &= 24\,(1+0.115\,Re^{0.802})/Re && \text{for } 2 < Re < 21 \\ &= 24\,(1+0.189\,Re^{0.632})/Re && \text{for } 21 < Re < 200. \end{aligned} \tag{5}$$

Previous researchers, including Ackley and Templeton (1979), solved eq 4 by numerical integration. They then calculated a global collection efficiency E, which is the fraction of water droplets in the path of the cylinder that collide with it. The global collection efficiency is calculated by finding the droplet trajectory that is tangent to the cylinder and determining the initial far-field distance from the centerline of the cylinder axis of that tangent trajectory. For example, if the initial far-field ordinate of the tangent trajectory is 0.75 units (with the cylinder radius representing one unit), then $E = 0.75$. For a distribution of water droplet sizes, the total collection efficiency is calculated by taking the global collection efficiency for each droplet size, multiplying by the fraction of the total liquid water content represented by that size, and summing over all droplet sizes in the distribution.

Solving the equation of motion in this manner allows time-dependent effects associated with the droplet trajectories to be included in the model. As ice accretes, the object changes shape and the flow field around the object changes. Ackley and Templeton (1979) modeled this effect by conforming the accretion to an elliptical shape. Since an analytical solution to the potential flow around an elliptical cylinder exists, they could determine the air flow field analytically. The drawback to this formulation, however, is that it is applicable only to objects with this simple cross section. Using numerical and transformation techniques, several researchers have developed models that can be applied to objects of arbitrary cross section, including airfoils or wires that rotate freely. Two possible approaches are the surface singularity method and the finite-element technique.

Surface singularity method

Lozowski and Oleskiw (1983) developed a computer model for airfoil icing that permitted simulation of the time-dependent growth of ice without runback on an arbitrary two-dimensional airfoil. The model can be used to predict the icing rate as well as accretion shape on airfoils when the accretion is dry. Dry accretion occurs when all of the impinging water droplets freeze upon impact so

there is no runback icing. This requires that the heat transfer from the airfoil surface is sufficient to freeze all of the impinging water droplets while maintaining the surface temperature below 0°C.

Lozowski and Oleskiw used a surface singularity method to determine the flow field around the two-dimensional airfoil. This technique divides the airfoil surface into a series of straight-line segments, and a constant but unknown vorticity is distributed along each. The stream function at any point external to the airfoil is then calculated by solving a set of linear algebraic equations for the unknown vorticity densities. The air velocity components are calculated at any desired point in the air stream by numerically differentiating the stream function. This approach has an advantage over other techniques in that the velocity components are determined at every point along the droplet trajectory, rather than being interpolated from a velocity field calculated at a discrete array of grid points. Lozowski and Oleskiw then applied the droplet equation of motion, which describes the motion of a spherical droplet in an accelerated air flow:

$$\frac{dV}{dt} = \underbrace{\frac{2(\rho_w-\rho_a)g}{(2\rho_w+\rho_a)}}_{\text{buoyancy}} - \underbrace{\frac{3C_d\rho_a|V-U|(V-U)}{4r(2\rho_w+\rho_a)}}_{\text{drag}} - \underbrace{\frac{9\rho_a\sqrt{(\nu/\pi)}}{(2\rho_w+\rho_a)}\int_{-\infty}^{t}\frac{dV\,d\tau}{d\tau\sqrt{(t-\tau)}}}_{\text{history}} \tag{6}$$

where g is gravitational acceleration and ν is the kinematic viscosity of air. The buoyancy term describes the vertical acceleration of the droplets due to gravity. The history term takes into account the fact that droplets are accelerating with respect to the flow and that, in fact, the problem is not steady-state. This equation also incorporates the induced droplet mass that results from the acceleration of air in the vicinity of an accelerating droplet. The buoyancy and history terms and induced mass effects are frequently dropped in many ice accretion models, resulting in the simplified form of this equation that was presented as eq 4. Lozowski and Oleskiw solved eq 6 numerically using a fourth-order Runge–Kutta–Fehlberg method, with the history term approximated by a combined numerical and analytical technique. Although their tests were not exhaustive, they indicated that the history term could be omitted without significantly affecting the results. The history term is most significant in cases with low collection efficiencies.

Lozowski and Oleskiw used local collection efficiencies to determine the rate of ice growth on each small segment of the airfoil surface. The advantage of this approach over earlier models (e.g. Ackley and Templeton 1979), which use a global collection efficiency to calculate the rate of ice growth in a predetermined shape, is its ability to model ice growth on objects with an arbitrary shape. The local collection efficiency $\beta(L)$ at any point on the airfoil surface is given by

$$\beta(L) = dY/dL \tag{7}$$

where L is the distance along the airfoil surface from the stagnation point and Y is the ordinate of the droplet starting point. The variables used in eq 7 are depicted in Figure 2. Lozowski and Oleskiw calculated the trajectories of 10–20 droplets with different starting ordinates and fit the resulting Y,L pairs to a cubic spline, which is differentiated to obtain the local collection efficiency. They calculated the accretion thickness h_i by

$$h_i = \dot{m}(L)\Delta t/\rho_i \tag{8}$$

where $\dot{m}(L) = U_0 W\beta(L)$ (9)

Δt = time period of accretion

ρ_i = ice density

W = liquid water content.

Using these equations a new airfoil surface shape is determined for each specified time interval.

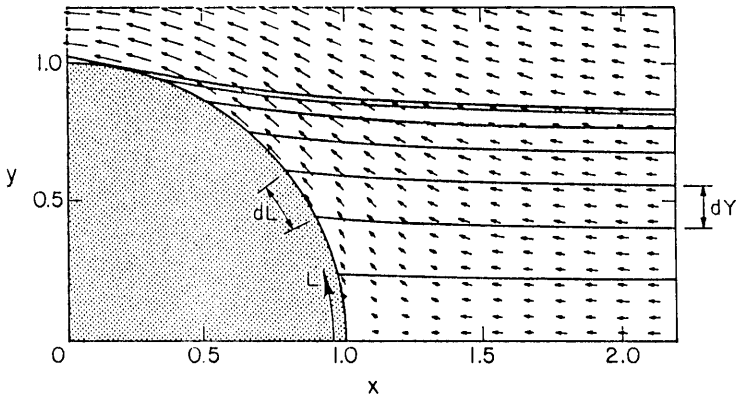

Figure 2. Air velocity field (arrows) and droplet trajectories (solid lines). Also shown are dL and dY used in eq 7. (After Lozowski and Oleskiw 1983.)

Finite-element technique

Finite-element models employ a piecewise approximation of the solution to the governing differential equations over the domain of interest. The primary advantage of this method is its ability to model irregularly shaped boundaries, even when the boundary is changing. Another advantage is that the size and shape of the finite elements can be varied, allowing greater accuracy in specific areas of the domain by using more elements of smaller size there. The finite-element method does have some disadvantages. The finite-element grid must be designed with the expected solution to the problem in mind. For example, in this problem, in regions where the air flow velocity gradients are large, the elements must be relatively small. Also, since the grid can be irregular, establishing the coordinates of each node can be tedious. This difficulty can be overcome by using a mesh-generating routine.

The basic steps that must be taken when using the finite-element method are as follows. First, the region of interest, in this case the air in front of the wire, must be divided into elements, either triangles or quadrilaterals. Next, the interpolating function to be used in each element is chosen. Polynomials are generally used because they can be easily differentiated and integrated. The third step is the derivation of the equations that describe the properties of each element. These equations are developed in matrix form, with the size of the matrix equal to the number of nodes in each element. In many simulations, as with our model, Galerkin's formulation is used. The fourth step is to assemble the element equations into a single global matrix of equations that describes the entire region of interest. This global matrix is then modified to account for the boundary conditions of the problem. The result is a system of simultaneous equations, with the number of equations equal to the number of nodes in the problem. Finally, the system of equations is solved using standard matrix decomposition procedures.

McComber (1981) and McComber and Touzot (1981) developed a numerical model of ice accretion using the finite-element method. The air and droplet velocity fields were calculated using triangular isoparametric quadratic elements. The finite-element method was chosen because the grid could be altered easily for different shapes. The droplet trajectories were determined by solving eq 4. The drag coefficient of the impinging water droplets was calculated using Beard and Pruppacher's (1969) formulation, shown previously as eq 5. McComber (1981) then used the droplet velocity field to determine the local collection efficiency β on the cylinder from the following relationship:

$$\beta = \bar{V} \cdot d\bar{l} \,/\, |d\bar{l}| \tag{10}$$

where $\bar{V}$ is the dimensionless droplet velocity at impact and $\bar{l}$ is the surface direction vector at the impact point. The mass flux of droplets impinging on the surface of the cylinder was determined by taking

the product of the local collection efficiency, the liquid water content, and the free stream velocity. Their simulation was for dry growth conditions only, and thus a thermodynamic balance at the surface of the cylinder was not required. Model results were compared with experimental results from wind tunnel tests, and qualitative agreement was found. However, the numerical model consistently overestimated the amount of ice accreted on the cylinders. Lozowski et al. (1985) commented on the definition of the collection efficiency shown in eq 10 and indicated that it is incorrect and tends to give larger collection efficiencies than actually occur. This may explain the overprediction of ice accretion mass in McComber (1981).

ACCRETION THERMODYNAMICS

Once the collection efficiency of the wire–ice system has been found, the next task is to determine whether the droplets freeze on impact. Several researchers (McComber 1981, Lozowski and Oleskiw 1983) assumed dry growth conditions in their models, in which all of the impinging water freezes at the point of impact. This is a good assumption at lower liquid water contents and lower air temperatures when the latent heat released during freezing is removed from the wire more quickly than it is released by the droplets freezing. However, at higher liquid water contents and at temperatures approaching 0°C, wet growth conditions frequently exist.

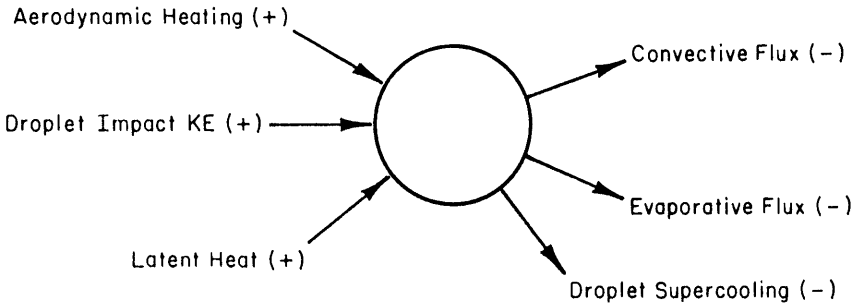

Figure 3. Heat balance at the freezing surface. (From Ackley and Templeton 1979.)

Modeling wet accretions is more difficult because only a fraction of the impinging water freezes on impact. The remaining water runs back toward the separation region of the wire, where it freezes or is shed. Ackley and Templeton (1979) calculated the heat balance at the surface of a cylinder during ice growth, basing their calculation on three conditions defined by whether all, a fraction, or none of the water froze on impact. Figure 3 shows the heat balance, indicating the direction of heat flow. The heat balance is the sum of the aerodynamic heating from compression of the flow, the kinetic energy of droplet impact, the latent heat released by droplet freezing, the convective and evaporative heat lost to the air flow, and the heat lost in warming supercooled droplets to 0°C:

$$Q = -hA\Delta t\left[\underbrace{(T_s - T_o)}_{\text{convective}} - \underbrace{\frac{R_s U_o^2}{2C_{pa}}}_{\text{aerodynamic}} + \underbrace{\frac{0.6L_v(E_s - E_o)}{PC_{pa}}}_{\text{evaporative}}\right]$$

$$-A\dot{m}C_{pw}\Delta t\left[\underbrace{\left(\frac{T_s C_{pi,w}}{C_{pw}} - T_o\right)}_{\text{supercooling}} - \underbrace{\frac{F_a L_f}{C_{pw}}}_{\text{latent}} - \underbrace{\frac{U_o^2}{2C_{pw}}}_{\text{kinetic}}\right] \qquad (11)$$

where Q = change in heat content per meter of wire
h = heat transfer coefficient
A = surface area of heat transfer per meter of wire
T_s = wire–ice surface temperature
T_o = ambient temperature
R_s = surface recovery factor ($0 < R_s < 1$)
C_{pa} = heat capacity of air
L_v = latent heat of vaporization of water
E_s = saturation vapor pressure of water over ice at T_s
E_o = saturation vapor pressure of water over ice at T_o
P = atmospheric pressure
C_{pw} = heat capacity of water
C_{pi} = heat capacity of ice
$C_{pi,w}$ = C_{pi} for $T_s < 0$ or C_{pw} for $T_s > 0$
L_f = latent heat of fusion of water
Δt = time increment
F_a = fraction of water accreted as ice.

In dry growth conditions, $T_s < 0°C$, $F_a = 1$ and C_{pi} is used in the supercooling term. In wet growth, $T_s = 0°C$ and F_a is between 0 and 1. For $T_s > 0°C$ none of the water accretes as ice, so $F_a = 0$ and C_{pw} is used in the supercooling term. The heat transfer coefficient is taken from Bosch's formulation (Boelter et al. 1965):

$$h = 31.01 U_o^{0.56} [273.16P / (1014T_f)]^{0.56} / D^{0.44} \tag{12}$$

where $T_f = 0.5(T_o + T_s)$.

In their analysis Ackley and Templeton (1979) followed Messinger (1953) and applied the appropriate temperature condition to solve for the change in heat content of the cylinder–ice system, which is then used to adjust the surface temperature and heat capacity C_{pc} of the wire and accretion during a time interval Δt using the following equations:

$$T_s' = T_s + Q/C_{pc} \tag{13}$$

$$C_{pc}' = C_{pc} + F_a C_{pi} \dot{m} A \Delta t \, . \tag{14}$$

Terms with a prime denote updated quantities. For $T_s = 0°C$ the fraction accreted is initially assumed to be unity, and if the resulting heat transfer is sufficient to freeze all of the water, the temperature drops below 0°C and dry accretion conditions apply. If not, an iterative procedure is initiated to determine the fraction accreted for the calculated change in heat content.

Other factors could be included in the thermodynamic model. Giedt (1949) showed from experimental work that the convective heat transfer varies by a factor of about two between the stagnation line and separation points on a circular cylinder for a Reynold's number based on the cylinder diameter ranging from 7×10^4 to 2.2×10^5. Lozowski et al. (1979) developed a model for icing with runback of unfrozen water on a fixed cylinder. In their model they used a convective heat transfer coefficient that varied with angle γ measured around the cylinder from the stagnation line. For a smooth cylinder

$$h = k_a [U_o \rho_a / (2\mu)]^{0.5} [1 - (\gamma/90°)^3] \tag{15}$$

where k_a is the molecular thermal conductivity of air. This relationship is based on the data of Achenbach (1974) and is valid for γ between 0° and about 80°. Another variable that affects heat

transfer is the roughness of the accretion surface. Preliminary measurements by Achenbach (1977) indicated that the convective heat transfer coefficient on a rough cylinder may be as much as twice that of a smooth one.

ICE ACCRETION PROFILE

The size and shape of the ice accretion are determined by the density of the accreting ice and the torsional flexibility of the wire. The eccentric weight of the accreted ice will cause the flexible wire to rotate as the ice accretes. According to Macklin (1962) the average density ρ_i of rime ice accreted on a rotating cylinder depends on the droplet size, the droplet impact velocity at the stagnation point, and the surface temperature of the accretion and is given by the following relationship:

$$\rho_i = 0.110\, R^{0.76}\ \text{Mg/m}^3 \tag{16}$$

where $R = -10^6 r V_o / T_s$ and V_o is the droplet impact speed at the stagnation line. This equation applies for R values between 0.8 and 10; Macklin suggested taking $\rho_i = 0.9\ \text{Mg/m}^3$ for larger values of R. Bain and Gayet (1983) provided a formula that approximates Macklin's curve for R between 10 and 60:

$$\rho_i = R/(R + 5.61)\ \text{Mg/m}^3, \tag{17}$$

For larger values of R, they took the accreted ice density to be $0.917\ \text{Mg/m}^3$.

As ice accretes on the windward side of a transmission line, the wire rotates in response to the eccentric weight. The average incremental rotation δ of a wire due to a total applied torque T is

$$T = K(\theta + \delta) \tag{18}$$

where K is the average wire torsional stiffness and θ is the wire rotation due to previous torque on the wire. Following Smith and Barker (1983) the torque on a wire due to an eccentric mass m_i is

$$T = m_i g d \sin[\tan^{-1}(d_x/d_y) + \delta] \tag{19}$$

where d_x = horizontal distance from the center of mass of the ice accretion to the wire center
d_y = vertical distance from the center of mass of the ice accretion to the wire center
$d = \left(d_x^2 + d_y^2\right)^{0.5}$

At equilibrium these torques will be equal. Assuming δ is small (say, less than 0.1 radian), then

$$\delta = (m_i g d_x - K\theta) / (K - m_i g d_y). \tag{20}$$

Thus, the incremental rotation of a wire depends on the stiffness and previous rotation of the wire as well as the mass and moment arm of the accretion.

The effective torsional stiffness of a wire fixed at both ends varies with distance from the fixed ends. In our model the wire rotation is calculated using the average torsional stiffness over the entire length of the wire. The rotation of a wire fixed at both ends and subject to a uniform torque T along its length L_w is

$$\theta(z) = T L_w (z/L_w)\,[1 - (z/L_w)]/(2GJ) \tag{21}$$

where G = wire shear modulus
J = wire polar moment of inertia

z = distance along the wire
L_w = wire length.

This equation is derived in Appendix A. The average stiffness can be found by determining the average rotation over the length of the wire:

$$\bar{\theta} = \frac{1}{L_w} \int_0^{L_w} \theta(z)\,dz = TL_w/(12GJ). \tag{22}$$

This gives an average wire stiffness of

$$K = 12GJ/L_w. \tag{23}$$

According to McComber (1983), for a typical aluminum stranded cable (Bersimis conductor with D = 3.5 cm), GJ = 351.4 Nm^2/rad. A 250-m-long wire, for example, will have an average torsional stiffness of 16.9 Nm/rad.

ICE AND WIND LOADS

The ultimate reason for modeling the ice growth on a transmission line during an icing event is to predict the horizontal and vertical forces exerted on the wire and its supporting structures. These forces are due to the combined effects of the weight of ice on the wire and any wind loading either during or following an icing event. Transmission line support structures are generally designed for a vertical compressive load imposed by the weight of the conductor and any accreted ice. The horizontal force due to the wind drag on an iced wire is difficult to quantify because it is a function of the size, shape and roughness of the accretion. Currently available models are capable of predicting the size and, in some cases, the shape of the accretion but not the roughness, which depends on the growth regime. The numerical simulation by Makkonen (1984b) indicates that the growth regime may change from wet growth to dry growth during an icing event of constant atmospheric conditions.

Assuming pseudostatic conditions, the total horizontal force due to wind drag on a length of wire with a circular cross section is (Blevins 1984)

$$F_x = 0.5 C_d \rho_a D_i L_w U_o^2 \tag{24}$$

where C_d = drag coefficient
ρ_a = density of air
D_i = diameter of the wire and ice accretion perpendicular to the airflow direction.

For smooth cylinders the drag coefficient is 1.2 at low Reynolds numbers and drops as low as 0.4 as the Reynolds number increases and the boundary layer becomes turbulent. However, ice accretions are typically neither cylindrical nor smooth. Assuming that the effects of roughness and shape may offset each other somewhat (the overall shape may be somewhat streamlined, and the increase in drag due to roughness may be partially offset by the drop in drag coefficient associated with the transition to a turbulent boundary layer), then taking C_d = 1 may not be unreasonable. Similarly the vertical force due to lift on the wire is (Blevins 1984)

$$F_l = 0.5 C_l \rho_a D_i L_w U_o^2 \tag{25}$$

where C_l is the lift coefficient. For airfoil cross sections the lift coefficient is proportional to the angle of attack α, for α less than approximately 15°. As the absolute angle of attack increases, the point of

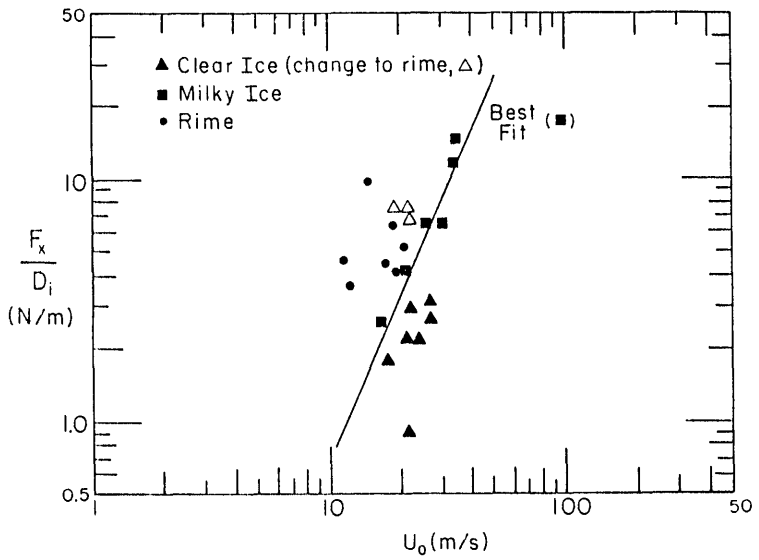

Figure 4. Horizontal force F_x *normalized to the accretion diameter* D_i *vs the wind speed normal to the wire for rime ice, milky ice and clear ice accretions. The best-fit line for the milky ice accretion is shown. (After Govoni and Ackley 1983.)*

flow separation moves forward until a critical angle of attack is reached where stall occurs. Then the magnitude of the lift coefficient decreases rapidly and the drag force increases.

The U.S. Army Cold Regions Research and Engineering Laboratory, in conjunction with the Mt. Washington Observatory, has been collecting simulated transmission line icing data since 1978 at the top of Mt. Washington, New Hampshire (Govoni and Ackley 1983). Instrumentation for the study consisted of a triaxial load cell mounted at one end of an 8-m wire capable of measuring vertical, horizontal and axial forces. They observed that the wire twisted as rime formed on its windward side, a consequence of the asymmetric weight of the accretion. As a result the final cross-sectional structure of the ice formation had a spiral pattern.

Govoni and Ackley (1983) analyzed the relationship between the drag force on the ice accretion, normalized to the diameter of the accretion, and the wind speed. Figure 4 shows a plot of F_x/D_i vs U_o for milky ice (high density with intermediate roughness), clear ice and rime. The plot indicates a good correlation between the normalized drag force and the wind speed for milky ice, implying a relatively constant drag coefficient throughout the icing event. However, when all the ice types are included, the correlation between the normalized drag force and the wind speed is weak, which was attributed to changes in the drag coefficient due to the changing shape of the accretion as ice collected. Figure 4 does indicate, however, an increase in the normalized drag force at a given wind speed for increasingly rough accretions.

According to McComber et al. (1983), Hydro-Quebec transmission lines are designed to withstand three loads: a wind load on bare wires corresponding to a wind speed of 137 km/hr (85 mph); an ice load consisting of a maximum radial ice thickness of 4.45 cm (1.75 in.) with no wind; and a combined load corresponding to a wind speed of 72 km/hr (45 mph) and a radial ice thickness of 3.18 cm (1.25 in.). The following method is used to calculate these design loads. The horizontal force due to wind drag on a bare wire is determined from eq 24, with $C_d = 1$ and $\rho_a = 1.3$ kg/m^3 to give

$$F_x = 0.65 D L_w U_o^2. \tag{26}$$

The horizontal force due to the combined effects of wind and ice are calculated using eq 26, with the exception that the ice accretion diameter D_i is used for D. This diameter is calculated from the ice

weight, assuming an ice density of 0.9 Mg/m^3. The vertical force F_y is obtained by adding the force due to the weight of accreted ice F_i and the force due to the weight of the wire. McComber et al. (1983) conducted wind tunnel experiments in which soft rime, hard rime and glaze were formed on rods. Horizontal and vertical forces on the iced rods were measured as a function of wind speed. In all cases the measured forces were about twice as big as the forces they calculated. It was determined that the measured horizontal forces were greater for two reasons: a) the actual rough asymmetric shapes of the ice accretions had drag coefficients larger than the assumed C_d = 1 and b) the soft and hard rime accretions had lower densities than the assumed 0.9 Mg/m^3 and therefore had larger diameters than were calculated from their weights, resulting in a further underestimate of the drag force. Also, it was found that in all cases except one, the measured lift force was negative and thus was equivalent to additional weight. They concluded that it will be difficult to predict aerodynamic forces on a power line because the final asymmetric shape of the accretion depends strongly on the history of its formation. The results of this study support the development of an ice accretion model to predict icing loads on wires with finite torsional rigidities.

COMPUTER MODEL

This study draws from previous icing models to construct an icing model for a wire of an arbitrary non-zero stiffness, allowing the size and shape of the ice accretion to be determined locally by the collection efficiency, the surface heat balance, the ice density and the wire stiffness. The model consists of a main program, where input and output are manipulated and all decisions occur, and thirteen subroutines, where all calculations are made. Figure 5 is a flow chart of the model, with each box representing a subroutine. In the first part of the model, the water droplet trajectories and the wire collection efficiency for a particular droplet size are determined. In the second part of the model, the heat balance calculations are carried out, the accretion profile is determined, and the rotation of the wire due to the asymmetric ice accretion is calculated.

The model starts by reading the model input, which consists of variables that define the problem to be solved, including droplet size, ambient air temperature, liquid water content, wind speed, wire diameter and stiffness, time step duration, and total simulation time. If a droplet size distribution is speci-

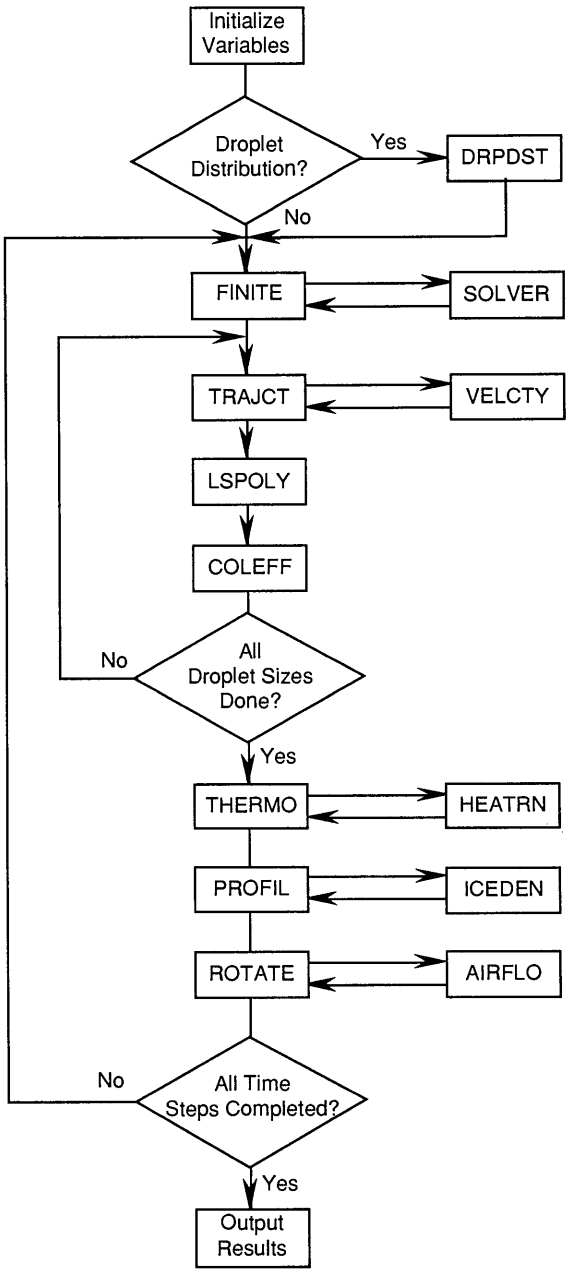

Figure 5. Flow chart of the wire icing program showing the main program, where the variables are initialized and the results are output, and the subroutines.

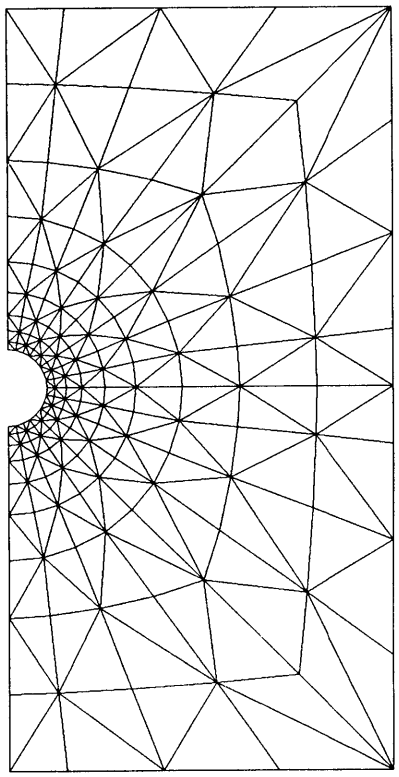

Figure 6. Finite-element mesh for the wire icing program.

fied, subroutine DRPDST is called to determine specific droplet size information. Subroutine FINITE calculates the air velocity field in the vicinity of the wire. The finite-element grid for this model was developed using MESH (Albert and Warren 1987), which is an automatic finite-element mesh generator. The mesh contains 170 nodes and 288 elements and has a half-bandwidth of 17 (Fig. 6). The nodes are numbered circumferentially starting from the outside boundary of the mesh and ending with the nodes on the wire–ice surface. Only the windward half of the wire is modeled, and the top, bottom and upstream boundaries of the mesh are taken far enough from the wire (10 wire radii) that the flow velocity there is not affected by the wire and takes on its uniform far-field value. Two data files are necessary to describe the grid. The first file contains the x and y coordinates of each node, and the second file is the incidence list, which relates the element number to the three nodes in counterclockwise order that define the element.

Laplace's equation (eq 1) describes the air flow around the wire. The method of weighted residuals and Galerkin's formulation were used to develop the equations comprising the local matrix for each element. The subroutine calculates the terms of the local matrix for each element and assembles the global matrix from the individual terms of the local matrices as they are being generated. The global matrix is relatively

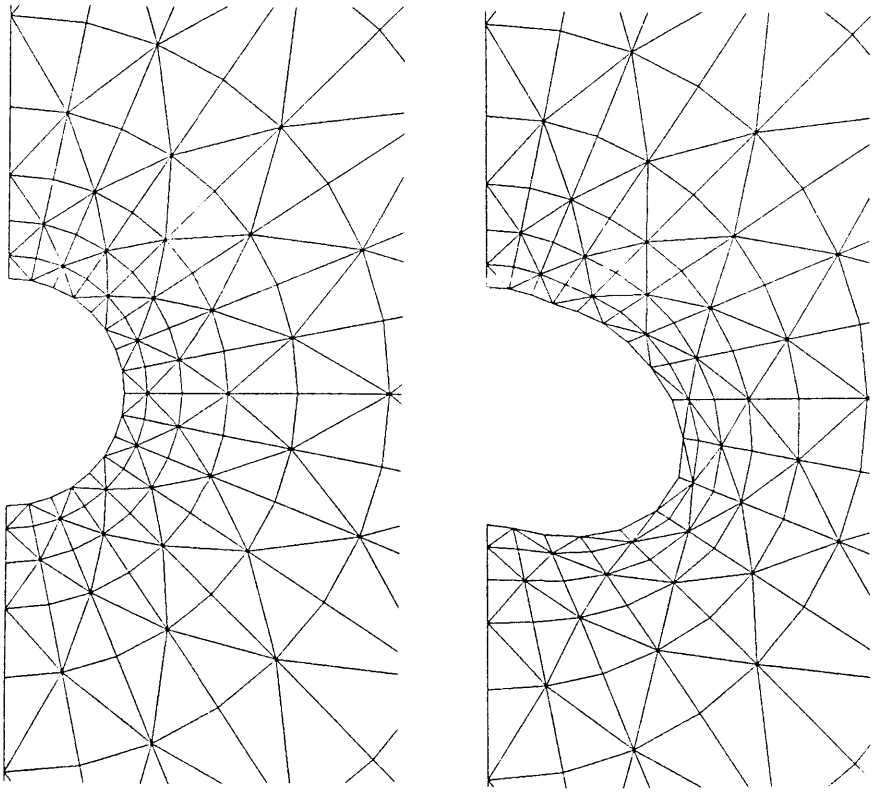

a. Undeformed mesh. *b. Deformed mesh after ice has accreted.*

Figure 7. Finite-element mesh close to the wire.

sparse and is stored in banded form. The boundary conditions are then enforced, and subroutine SOLVER is called to solve the system of equations represented by the global matrix. SOLVER is a commercially available routine that solves a system of equations in asymmetric banded form using a decomposition procedure. Finally the x and y components of the air velocity are determined for each element using eq 2.

Subroutine FINITE incorporates a movable boundary adjacent to the wire to allow for the accretion of ice on the wire. Figure 8 shows how the boundary nodes and the first three rows of the finite-element grid move as the ice grows. The mesh can deform to accept an ice accretion thickness up to about 1.5 times the wire radius. Since ice growth causes a change in the air flow around the accretion, a new velocity field is calculated during each time step.

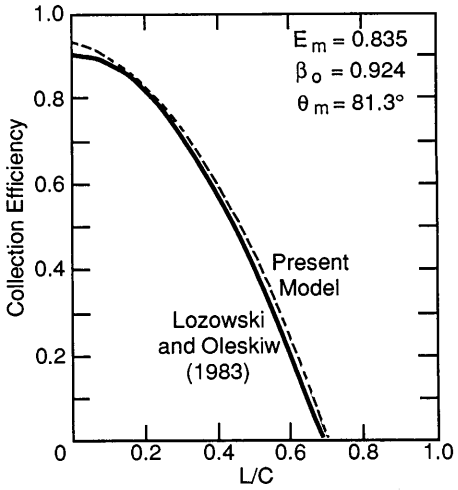

Figure 8. Comparison of the local collection efficiency calculated by the present model with that of Lozowski and Oleskiw (1983).

Subroutine TRAJCT determines the point of impact on the wire of water droplets in the air stream. This is accomplished by starting with a droplet at the right boundary of the finite-element grid, applying the equation of droplet motion (eq 4), using the drag coefficient calculated from eq 5, and calculating a new position and velocity of the droplet 0.1 dimensionless time units later. By repeating this procedure, the droplet is tracked until it collides with the wire or completely misses it. A droplet is then inserted at a new starting location 0.025 units (1 unit = 1 cylinder radius) below the starting location of the first droplet, and this droplet is tracked until it collides with the wire. This procedure is repeated while moving the starting location down the upstream boundary until the droplet misses the bottom of the wire.

Subroutine TRAJCT periodically calls on subroutine VELCTY to determine the air stream velocity at the current droplet position. Subroutine VELCTY determines which finite element contains the droplet by using the following optimized technique. The subroutine first determines whether the droplet is in the same element as it was previously. If not, it checks the other elements by testing first whether the droplet is within an x and y tolerance of it. If it is, it calculates the areas of three subtriangles formed by the droplet position and two nodes of the element in question. If each of these areas is positive, the droplet is contained in that finite element. Using the velocities calculated in subroutine FINITE, the x and y components of the air velocity at the new droplet position are determined.

TRAJCT produces a set of up to 80 pairs of numbers, each pair consisting of Y, the ordinate of the droplet starting trajectory, and L, the distance along the wire surface from the impact point to the stagnation point (Fig. 2). Once the path of a particular droplet is calculated, the subroutine finds the point of impact of the droplet on the wire–ice surface. The first step is to determine whether the droplet is past the wire stagnation point, and therefore within range of a potential impact, or above the top or below the bottom of the wire, and therefore cannot collide with the wire. The subroutine then determines which segment of the wire–ice surface the droplet is near by comparing the x and y coordinates of the wire–ice boundary nodes with the coordinates of the current droplet position. If the droplet has collided with the wire, the intersection of the wire–ice surface segment and the last trajectory line segment is determined. If not, another iteration is performed to move the droplet closer to the wire. Finally, L is calculated by summing the segment lengths between the impact point and the stagnation point. This procedure is repeated until a set of points is generated relating Y, the starting ordinate, and L, the distance along the wire–ice surface from the stagnation point to the impact point, for up to 80 starting points. This information is passed on to subroutine LSPOLY.

LSPOLY is a commercial program that uses a least-squares routine to fit the set of data points

obtained from TRAJCT to a third-order polynomial. The coefficients of the cubic equation are passed on to subroutine COLEFF. Subroutine COLEFF uses the cubic equations describing the trajectory data to calculate the local collection efficiency along the wire–ice surface. The starting ordinate associated with each of the boundary nodes is determined from the cubic relationship, and eq 7 in difference form is used to calculate the collection efficiency for each surface segment. Figure 8 is a comparison of the local collection efficiency calculated in the present model with that of Lozowski and Oleskiw (1983). The agreement is excellent except near the stagnation point. The difference is probably due to the discrete numerical solution for the air flow field in this model. The local collection efficiencies, along with the wind speed and the liquid water content, are used to calculate the mass flux of water to each surface segment. The mass of ice accreted on each segment is determined by considering the thermodynamic processes occurring at the surface of the accretion in subroutine THERMO.

THERMO determines how much of the impinging water mass freezes. The computer code used in THERMO was adapted from the model developed by Ackley and Templeton (1979), which relied on a heat balance at the freezing surface to determine whether all, a fraction, or none of the impinging water freezes. The primary difference between the thermodynamic model developed by Ackley and Templeton (1979) and this model is that the former treats the heat balance globally, while here it is calculated locally. THERMO analyzes the heat balance at each of the 16 surface segments, calling subroutine HEATRN to determine the convective heat transfer coefficient. The amount of ice accreted also depends on the mass flux of water to the surface segment, the time step duration, the surface segment length, and the fraction of the incident water mass that freezes and is calculated using eq 11 and 12. Higher collection efficiencies imply more incident water and a greater heat flux to the wire–ice surface. This results in a surface temperature pattern of warmer temperatures near the stagnation point than at the top and bottom of the wire (Fig. 9). This variation in wire–ice surface temperature affects the density and thus the volume of the accretion. Also, by calculating the surface temperature distribution, the transition from dry growth to wet growth can be investigated. Since the maximum local collection efficiency of the wire–ice surface occurs near the stagnation point, one would expect the transition to wet growth to occur there first. By performing a mass balance of the runback water that is created during wet growth conditions, this phenomenon could be modeled. Lozowski et al. (1983) included freezing of runback water in the icing of a non-rotating cylinder. Their model assumes symmetric ice growth about the stagnation line, which is appropriate for the icing of a non-rotating cylinder subject to high winds. For the lower wind speeds and finite-stiffness wires considered in this model, determining the direction of flow of the unfrozen water is more complicated and remains for future work.

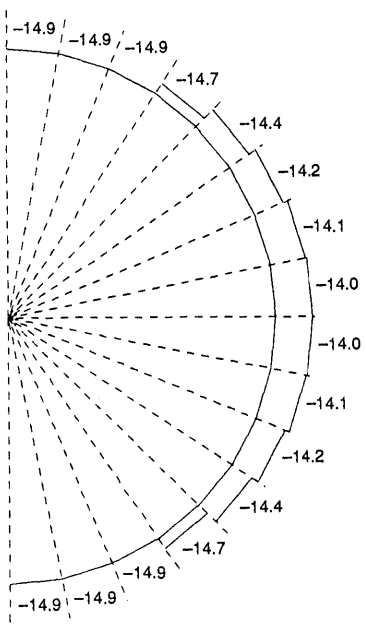

Figure 9. Example of wire–ice surface temperatures calculated by subroutine THERMO for an air temperature of –15 °C.

The profile of the accreted layer is calculated in subroutine PROFIL, which calls on subroutine ICEDEN to determine the density of the ice (using eq 16 and 17) in each of the sectors of the accretion layer. Subroutine PROFIL determines the thickness of ice accreted on each surface segment during a time step. The accretion thickness varies along the wire–ice surface because of variations in local collection efficiency, fraction of incident water frozen, and ice density. It was assumed that growth is perpendicular to the orientation of each of these segments, so subroutine PROFIL distributes the mass accreted on each surface segment in a trapezoidal cross-sectional shape, as shown in Figure 10a. The coordinates of these trapezoids are then passed to subroutine ROTATE, where the torque due to the asymmetric ice weight is calculated.

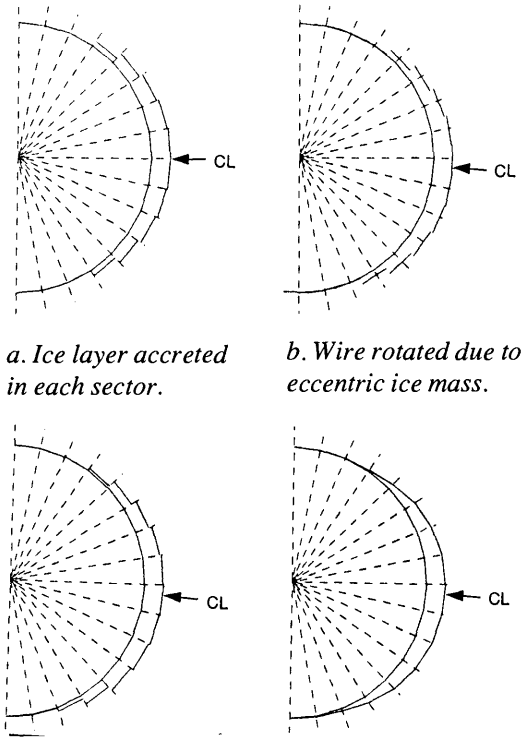

a. Ice layer accreted in each sector.

b. Wire rotated due to eccentric ice mass.

c. New ice profile in each sector.

d. Smoothed ice accretion profile.

Figure 10. Steps in the calculation of the accreted ice layer profile.

The purpose of subroutine ROTATE is to calculate the torque created by the accretion of ice on the windward side of the wire, the amount of rotation due to this torque, and the coordinates of the finite-element boundary nodes after rotation. Using eq 20, ROTATE calculates the incremental rotation at the end of each time step (Fig. 10b). The post-rotation cross-sectional area of the new ice accretion layer in each sector is computed and distributed in a trapezoidal shape, as was done in PROFIL (Fig. 10c). ROTATE then calculates a continuous accretion boundary by averaging the adjacent end point coordinates of each pair of the new sector boundaries (Fig. 10d).

RESULTS

The results of 13 icing simulations are described in this section. The simulations investigate the variation in vertical (gravitational) and horizontal (wind) load on a 3.5-cm-diameter wire due to variations in the atmospheric conditions and the transmission line design. The simulations are carried out for one hour. A typical icing event is represented by the default case for which U_0 = 10 m/s, T_0= –15°C, W = 0.0005 kg/m^3 and r = 17 μm. The default wire properties are taken as D = 3.5 cm, L_w=250 m and K = 16

Table 1. Results of icing simulations. For each simulation the atmospheric and wire variables are given as well as the final wire rotation angle, the accreted mass per unit length of wire, the vertical load on the wire span, the horizontal load on the wire span, and the accretion diameter perpendicular to the wind. The default case is shown first. In the other cases the parameter values that differ from those in the default case are in bold type.

Input variables						*Results*				
Atmospheric				*Wire*						
r (μm)	W (g/m^3)	T_o (°C)	U_o (m/s)	K (Nm/rad)	L_w (m)	θ (deg)	m_i/L_w (kg/m)	F_i (N)	F_x (N)	D_i (cm)
17	0.5	–15	10	16	250	49	0.29	701	645	3.9
17	0.5	**–5**	10	16	250	5	0.28	678	603	3.7
17	0.5	**–25**	10	16	250	53	0.28	692	708	4.1
17	0.5	–15	**20**	16	250	106	0.82	2019	3500	5.2
17	0.5	–15	**30**	16	250	146	1.50	3668	8973	5.9
17	**0.25**	–15	10	16	250	24	0.14	353	603	3.5
17	**0.75**	–15	10	16	250	72	0.44	1073	745	4.4
10	0.5	–15	10	16	250	23	0.12	292	605	3.6
13	0.5	–15	10	16	250	6	0.19	477	608	3.6
17	0.5	–15	10	**32**	250	27	0.28	676	605	3.6
17	0.5	–15	10	**8**	250	81	0.30	740	713	4.2
17	0.5	–15	10	**32**	**125**	14	0.27	332	301	3.5
17	0.5	–15	10	**8**	**500**	120	0.31	1514	1460	4.3

Nm/rad. The final cross-sectional accretion diameter perpendicular to the wind, the rotation angle, the mass of accretion per meter of wire, the ice load and the wind load are shown in Table 1 for all 13 simulations. The wind load is calculated using eq 20 with $C_d = 1$. The accretion profiles are compared in Figure 11.

Atmospheric variables

The ambient air temperature was varied from the default value of –15°C to –5 and –25°C. The effect of these different air temperatures is to change the density of the accretion, which alters the accretion profile and thus the moment arm causing rotation. At the higher air temperatures, the surface temperature of the accretion approaches 0°C near the stagnation point and not all the incoming liquid water freezes. Assuming this water is shed rather than running back and freezing gives a lower accretion mass than in the colder simulations. Table 1 indicates that higher ambient temperatures lead to slightly lower ice and wind loads on the transmission line. The accretion profiles are shown in Figure 11a.

The wind speed was varied from the default value of 10 m/s to 20 and 30 m/s. The increased wind speed increases the collection efficiency of the wire and the flux of water droplets past the wire, resulting in greatly increased ice and wind loads on the wire. The low-wind-speed accretion has a lower surface temperature and is likely to be rougher than the ice accreted at the higher wind speeds. The accretion roughness will also affect the wind load on the wire, but this effect has not been quantified. The accretion profiles are shown Figure 11b.

The liquid water content was varied from its default value of 0.0005 kg/m^3 to 0.00025 and 0.00075 kg/m^3. The ice load is roughly proportional to the liquid water content for these simulations. The wind load increases somewhat with liquid water content because of the associated increase in the cross-sectional diameter of the accretion. The accretion profiles are shown in Figure 11c.

The droplet radius was varied from its default value of 17 μm to 10 and 13 μm. The decreased collection efficiency for the smaller droplet sizes gives smaller ice loads and somewhat smaller wind loads. The accretion profiles are shown in Figure 11d.

Wire variables

The average wire stiffness was varied from its default value of 16 Nm/rad to 8 and 32 Nm/rad. This was

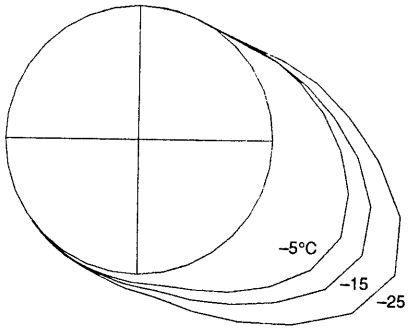

a. Air temperatures –5, –15 and –25°C.

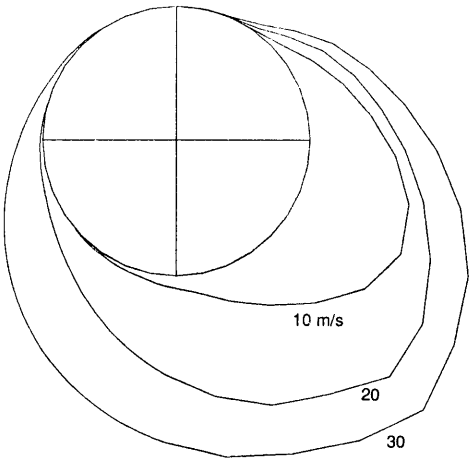

b. Wind speeds 10, 20 and 30 m/s.

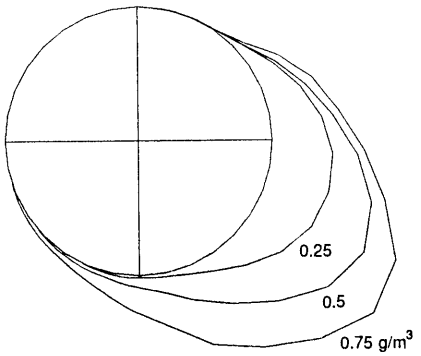

c. Liquid water contents 0.25, 0.5 and 0.75 g/m^3.

Figure 11. Final ice accretion profiles for 13 model simulations. For the default case, air temperature = –15°C, wind speed = 10 m/s, liquid water content = 0.5 g/m^3, drop size = 17 μm, wire stiffness = 16 Nm/rad, wire length = 250 m. For the other cases one variable at a time was changed. Each figure shows the default case along with two other cases.

assumed to have been done by using different materials in manufacturing the wire, without changing the wire diameter. The wire stiffness affects the amount of rotation for a given accreted mass of ice, which affects the accretion collection efficiencies and the final accretion profile. The ice and wind loads decrease slightly as the wire stiffness increases. The accretion profiles are shown in Figure 11e.

Changing the span of the transmission line between support structures changes the average stiffness as well as the length of the wire (eq 29). The wire length was varied from its default value of 250 m to 125 and 500 m. Assuming the same wire shear modulus and polar moment of inertia gives wire stiffnesses of 8 and 32 Nm/rad, respectively, for these cases. The longer, more-flexible wire accretes more ice and rotates through a larger angle than the stiffer wires. This effect is compounded in the ice and wind load calculations by the greater wire length over which the ice collects, resulting in greatly increased vertical and horizontal loads on support structures. The accretion profiles are shown in Figure 11f.

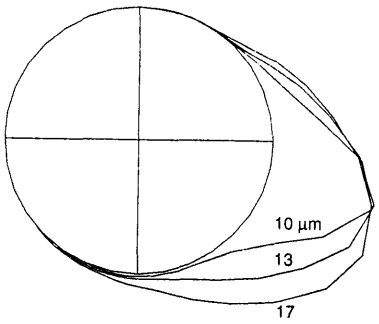

d. Drop sizes 10, 13 and 17 μm.

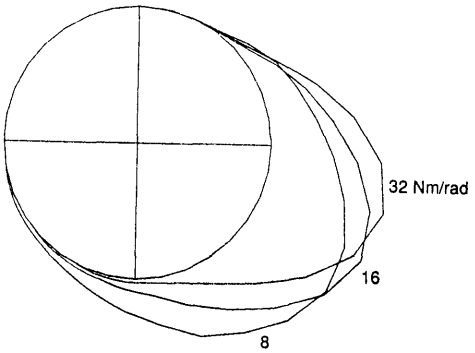

e. Wire stiffnesses 8, 16 and 32 Nm/rad.

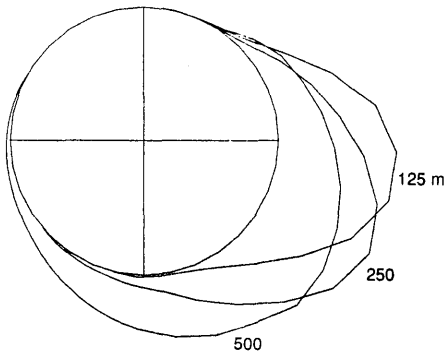

f. Wire lengths 125, 250 and 500 m with corresponding stiffnesses.

Figure 11 (cont'd). Final ice accretion profiles for 13 model simulations. For the default case, air temperature = –15 °C, wind speed = 10 m/s, liquid water content = 0.5 g/m^3, drop size = 17 μm, wire stiffness = 16 Nm/rad, wire length = 250 m. For the other cases one variable at a time was changed. Each figure shows the default case along with two other cases.

Summary

These simulations quantify the dependence of ice and wind loads on atmospheric varibles and on design variables of the wire and support structures. Ice and wind loads on a transmission line increase with increasing wind speed, liquid water content and drop size. The wind load increases somewhat with decreasing air temperature, but the ice load is not sensitive to air temperature variations. Ice and wind loads decrease with increasing wire stiffness but only slightly. However, these loads increase markedly with increasing wire length and the associated decrease in average wire stiffness.

CONCLUSIONS

After identifying a potential or existing ice accretion problem, the design engineer must choose between designing for a particular icing event at the location of interest or relocating the transmission line.

Transmission line relocation should always be the first option investigated because avoiding a foreseeable problem is the easiest way to solve it. This may be an attractive option if the line traverses terrain where atmospheric icing is a problem for only a short distance, such as a mountain pass. It may be possible to adjust the transmission line orientation and location in a pass to avoid the full impact of prevailing winds. The wind speed has a great effect on the ice load and the wind load because of

the increase in collection efficiency at higher wind speeds, the increased flux of droplets past the wire, and the dependence of wind drag on the square of the wind speed. In many cases, however, right-of-way acquisition may preclude relocation of the line. The transmission line may also traverse open and exposed areas for miles, in which case relocation is simply not an option. If the problem cannot be avoided, the design of the line and the support structures must either take into account the increased loading associated with atmospheric icing or bear the losses associated with increased maintenance associated with icing storms and the loss of revenue from customers during power outages. If a severe icing storm occurs only once in 20 years, this may be an attractive option.

The computer simulations indicate that, with regard to structural design, the length or stiffness of a transmission line can be changed to decrease the ice and wind loads on the wire and support structures due to an icing storm. The wire stiffness can be increased in practice by increasing the diameter of the wire (which also decreases the wire collection efficiency), by increasing the shear modulus of the material in the wire, or by using phase spacers. Phase spacers are short rigid cylinders made from an insulating material such as fiberglass and are installed midspan with a primary purpose of preventing two phases of the transmission system from touching and shorting out. These spacers can be designed to prevent the wire from rotating where they attach, which effectively increases the average wire stiffness. An additional advantage is that these spacers can be installed on transmission lines already in service. It must be emphasized that model results indicate only a 5–10% reduction in the ice load or wind load on the wire and support structures associated with doubling the average wire stiffness. However, the reduction in support structure ice and wind loads associated with reducing the wire length (which also causes the average wire stiffness to increase) is roughly the same as the length reduction. This effect is primarily due to the decreased length of wire between supports. In the wire simulations presented earlier, for example, a reduction in the wire length from 250 m to 125 m caused a 53% reduction in both the ice and wind loads on the support structures.

These results are from a limited number of simulations for which the duration of the icing event was only one hour, while many icing storms last hours or even days. They require confirmation through field or wind tunnel testing before confident design changes can be made for planned or existing transmission lines. It must also be considered that changing the wire stiffness or support structure separation may not be practical from the standpoint of designing the line for its primary purpose.

FUTURE WORK

Future work can be divided into three areas: modeling, laboratory studies and field studies. The limitations of modeling are the physical simplifications that must be made to quantify many of the factors that contribute to the complex phenomenon of atmospheric ice accretion. Laboratory studies are limited by the sophisticated hardware that must be employed to simulate an icing event. Field studies are difficult because of the harsh conditions associated with icing storms and the infrequency of their occurrence. However, more laboratory and field work is required to verify results obtained in this and other similar computer modeling efforts.

Future modeling studies can be improved in two ways: improving the thermodynamic calculations at the surface of the accretion and improving the calculation of the wind load. Many of the ideas presented in this study require verification, especially the concept of the accretion having a variable temperature distribution on its surface. A method of quantifying the change in convective heat transfer coefficient along the surface of an accretion should be investigated. To improve the accuracy of wind load calculations, future work should include a parameterization of the accretion roughness and its effect on the drag coefficient. Future work might also include an analysis of the fate of the unfrozen water on the surface of a glaze ice accretion.

Laboratory studies would be useful in verifying the results presented in this study, especially the variation in temperature on the surface of the accretion. Wind tunnel experiments could be set up to measure the variation in convective heat transfer coefficient on the surface of a cylinder with a

noncylindrical cross section to extend the work of Achenbach (1974). Measurements of the drag coefficient associated with different roughness heights would also be useful.

Finally, assumptions and conclusions should be verified in the field. Continued measurements of ice accretion and wind loads on actual transmission lines by Ontario Hydro Research (Krishnasamy 1983) would be of great value. In the final analysis, field inspections and measurements by technical and nontechnical personnel will probably contribute the most to our understanding of the ice accretion process and improved engineering design.

LITERATURE CITED

Achenbach, E. (1974) Heat transfer from smooth and rough surfaced circular cylinders in a cross flow. In *Proceedings of the 5th International Heat Transfer Conference, Tokyo*, p. 229–233.

Achenbach, E. (1977) The effect of surface roughness on the heat transfer from a circular cylinder to the cross flow of air. *International Journal of Heat and Mass Transfer*, **20**: 359–369.

Ackley, S.F. and M.K. Templeton (1979) Computer modeling of atmospheric ice accretion. USA Cold Regions Research and Engineering Laboratory, CRREL Report 79-4.

Albert, M.R. and J.L. Warren (1987) An automatic finite element mesh generator. USA Cold Regions Research and Engineering Laboratory, CRREL Report 87-18.

Bain, M. and J.F. Gayet (1983) Contribution to the modeling of the ice accretion process: Density variation with the impacted surface angle. In *Proceedings of the First International Workshop on Atmospheric Icing on Structures, Hanover, New Hampshire*. USA Cold Regions Research and Engineering Laboratory, Special Report 83-17, p. 13–20.

Batchelor, G.K. (1970) *An Introduction to Fluid Dynamics*. Cambridge: Cambridge University Press.

Battan, L.J. (1962) *Cloud Physics and Cloud Seeding*. New York: Doubleday and Co.

Beard, K.V. and H.R. Pruppacher (1969) A determination of the terminal velocity and drag of small water drops by means of a wind tunnel. *Journal of Atmospheric Science*, **26**(5): 1066–1072.

Blevins, R.D. (1984) *Applied Fluid Dynamics Handbook*. New York: Van Nostrand Rheinhold.

Boelter, L.M.K., V.H. Cherry, H.A. Johnson and R.C. Marinelli (1965) *Heat Transfer Notes*. New York: McGraw-Hill.

Brun, R.J. (1957) Icing problems and recommended solutions. AGARDograph 16, NATO.

Giedt, W.H. (1949) Investigations of variation of point unit heat-transfer coefficient around a cylinder normal to an air stream. *Transactions of the ASME*, **17:** 375–381.

Govoni, J.W. and S.F. Ackley (1983) Field measurements of combined icing and wind loads on wires. In *Proceedings of the First International Workshop on Atmospheric Icing on Structures, Hanover, New Hampshire*. USA Cold Regions Research and Engineering Laboratory, Special Report 83-17, p. 205–216.

Hess, J.L. and A.M.O. Smith (1967) Calculation of potential flow about arbitrary bodies. *Progress in Aeronautical Science*, vol. 8.

Krishnasamy, S.G. (1983) Measurement of ice accretion on overhead transmission line conductors. In *Proceedings of the First International Workshop on Atmospheric Icing on Structures, Hanover, New Hampshire*. USA Cold Regions Research and Engineering Laboratory, Special Report 83-17, p. 291–298.

Langmuir, I. and K.B. Blodgett (1946) A mathematical investigation of water droplet trajectories. In *Collected Works of Irving Langmuir*. New York: Pergamon Press, p. 348–393.

Lozowski, E.P., J.R. Stallabrass and P.F. Hearty (1979) The icing of an unheated non-rotating cylinder in liquid water droplet-ice crystal clouds. National Research Council of Canada, Division of Mechanical Engineering, Laboratory Technical Report LTR-LT-96.

Lozowski, E.P., J.R. Stallabrass and P.F. Hearty (1983) The icing of an unheated, nonrotating cylinder. Part I: A simulation model. *Journal of Climate and Applied Meteorology*, **22**(12): 2053–2063.

Lozowski, E.P. and M.M. Oleskiw (1983) Computer modeling of time-dependent rime icing in the atmosphere. USA Cold Regions Research and Engineering Laboratory, CRREL Report 83-2.
Lozowski, E.P., K.J. Finstad and E.M. Gates (1985) Comments on calculation of the impingement of cloud droplets on a cylinder by the finite element method. *Journal of the Atmospheric Sciences*, **42**(3): 306–307.
Macklin, W.C. (1962) The density and structure of ice formed by accretion. *Quarterly Journal of the Royal Meteorological Society*, **88**: 30–50.
Makkonen, L. (1984a) Atmospheric icing on sea structures. USA Cold Regions Research and Engineering Laboratory, Monograph 84-2.
Makkonen, L. (1984b) Modeling of ice accretion on wires. *Journal of Climate and Applied Meteorology*, **2**: 929–939.
Mallory, J.H. and D.C. Leavengood (1983) Extreme glaze and rime ice loads in southern California. Part I: Rime. Southern California Edison Company. In *Proceedings of the First International Workshop on Atmospheric Icing on Structures, Hanover, New Hampshire*. USA Cold Regions Research and Engineering Laboratory, Special Report 83-17, p. 299–308.
McComber, P. (1981) Numerical simulation of ice accretion using the finite element method. In *POAC 81: Proceedings, 6th International Conference on Port and Ocean Engineering under Arctic Conditions, 27–31 July, Quebec, Canada*. Université Laval, vol. 2, p. 1047–1056.
McComber, P. (1983) Numerical simulation of ice accretion on cables. In *Proceedings of the First International Workshop on Atmospheric Icing on Structures, Hanover, New Hampshire*. USA Cold Regions Research and Engineering Laboratory, Special Report 83-17, p. 51–58.
McComber, P. and G. Touzot (1981) Calculation of the impingement of cloud droplets in a cylinder by the finite element method. *Journal of the Atmospheric Sciences*, **38**(5): 1027–1036.
McComber, P., J.L. Laforte, D. Bouchard and D. Nguyen (1982) Ice measurements on fixed and rotating cylinders. Université du Quebec a Chicoutimi (unpublished report).
McComber, P., R. Martin, G. Morin and L. Vo Van (1983) Estimation of combined ice and wind load on overhead transmission lines. In *Proceedings of the First International Workshop on Atmospheric Icing on Structures, Hanover, New Hampshire*. USA Cold Regions Research and Engineering Laboratory, Special Report 83-17, p. 143–154.
Messinger, B.L. (1953) Equilibrium temperature of an unheated icing surface as a function of airspeed. *Journal of Aeronautical Science*, **20**: 29–42.
Smith, B.W. and C.P. Barker (1983) Icing of cables. In *Proceedings of the First International Workshop on Atmospheric Icing on Structures, Hanover, New Hampshire*. USA Cold Regions Research and Engineering Laboratory, Special Report 83-17, p. 41–50.
Tattleman, P. (1983) Surface icing research at the Air Force Geophysics Laboratory. In *Proceedings of the First International Workshop on Atmospheric Icing on Structures, Hanover, New Hampshire*. USA Cold Regions Research and Engineering Laboratory, Special Report 83-17, p. 195–204.
Theodorson, T. and J.E. Garrick (1932) General potential theory of arbitrary wind sections. NACA Report 452, Washington, D.C.
Volterra, E. and J.H. Gaines (1971) *Advanced Strength of Materials*. Englewood Cliffs, New Jersey: Prentice Hall, Inc.

APPENDIX A: DETERMINING THE ANGLE OF TWIST ALONG A CYLINDER FIXED AT BOTH ENDS SUBJECT TO A DISTRIBUTED TORQUE ALONG ITS LENGTH

First determine the angle of twist along a cylinder fixed at one end and subject to a concentrated torque at $z = L$:

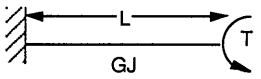

From Volterra and Gaines (1971, p. 217) the angle of twist at a distance z from the fixed end is

$$\theta(z) = zT/GJ \tag{A1}$$

where G = shear modulus
J = polar moment of inertia
T = applied torque.

The torsional stiffness K of the cylinder is the ratio between the applied torque and the rotation angle

$$K = GJ/z. \tag{A2}$$

Next determine the angle of twist along a cylinder fixed at both ends subject to a concentrated torque at $z = l$.

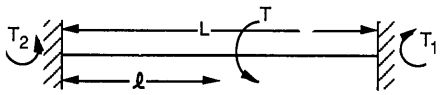

The resisting moments at the fixed ends must satisfy $T_1+T_2 = T$. At $z = l$ the angles of twist must match: $\theta_1 = T_1 l/GJ$ must equal $\theta_2 = T_2(L-l)/GJ$.

Solving for T_1 gives

$$T_1 = (L-l)T/L \tag{A3}$$

and

$$\theta(l) = (L-l)lT/GJI \tag{A4}$$

How does the twist angle depend on z? It must vary linearly on either side of the concentrated torque as in eq A1 and be zero at the fixed ends, so

$$\theta(z) = (L-l)zT/GJL \qquad z \le l$$
$$\theta(z) = l(L-z)T/GJL \qquad z \ge l. \tag{A5}$$

Now determine the angle of twist along a cylinder fixed at both ends subject to a distributed torque t per unit length along the whole length. First look at a small element dz:

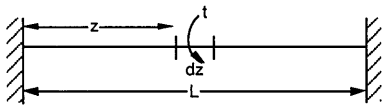

The angle of twist at z due to the applied torque t over the length dz is (using eq A4):

$$d\theta(z) = (L-z)ztdz/GJL. \tag{A6}$$

The twist angle at any other point z_o due to that applied torque is (using eq A5)

$$d\theta(z_o) = (L-z)z_o tdz/GJL \qquad z_o \le z$$
$$d\theta(z_o) = z(L-z_o)tdz/GJL \qquad z_o \ge z. \tag{A7}$$

The distributed torque t per unit length is applied over the whole length of the cylinder, so eq A7 can be integrated over z to get the total twist angle at z_o:

$$\theta(z_o) = \int_0^{z_o} \frac{t(L-z_o)z}{GJL}\,dz + \int_{z_o}^{L} \frac{tz_o(L-z))}{GJL}\,dz \tag{A8}$$

which gives

$$\theta(z_o) = (tL)\,L(1-z/L)\,(z/L)/2GJ. \tag{A9}$$

This is eq 21 in the main text.

REPORT DOCUMENTATION PAGE

Form Approved
OMB No. 0704-0188

1. AGENCY USE ONLY (Leave blank)	2. REPORT DATE	3. REPORT TYPE AND DATES COVERED
	February 1991	

4. TITLE AND SUBTITLE

Computer Model of Atmospheric Ice Accretion on Transmission Lines

5. FUNDING NUMBERS

PE: 4A161102AT24
TA: FS
WU: 005

6. AUTHORS

Kathleen F. Jones and Kurt Z. Egelhofer

7. PERFORMING ORGANIZATION NAME(S) AND ADDRESS(ES)

U.S. Army Cold Regions Research and Engineering Laboratory
72 Lyme Road
Hanover, New Hampshire 03755-1290

8. PERFORMING ORGANIZATION REPORT NUMBER

CRREL Report 91-3

9. SPONSORING/MONITORING AGENCY NAME(S) AND ADDRESS(ES)

Office of the Chief of Engineers
Washington, D.C. 20314-1000

10. SPONSORING/MONITORING AGENCY REPORT NUMBER

11. SUPPLEMENTARY NOTES

12a. DISTRIBUTION/AVAILABILITY STATEMENT

Approved for public release; distribution is unlimited.

Available from NTIS, Springfield, Virginia 22161.

12b. DISTRIBUTION CODE

13. ABSTRACT (*Maximum 200 words*)

Atmospheric ice accretions on transmission lines cause increased gravity and wind loads on the lines. In regions subject to icing conditions, transmission line design must take these loads into account. This report describes a numerical model for determining the accretion of ice on transmission lines. The eccentric ice load causes a gradual rotation of the flexible conductor, which affects the shape and size of the accretion. The sensitivity of the gravity and wind load on the conductor to both atmospheric and structural variables is examined.

14. SUBJECT TERMS

Computer models | Ice accretion | Transmission lines

15. NUMBER OF PAGES

31

16. PRICE CODE

17. SECURITY CLASSIFICATION OF REPORT	18. SECURITY CLASSIFICATION OF THIS PAGE	19. SECURITY CLASSIFICATION OF ABSTRACT	20. LIMITATION OF ABSTRACT
UNCLASSIFIED	UNCLASSIFIED	UNCLASSIFIED	UL

NSN 7540-01-280-5500

☆U.S. GOVERNMENT PRINTING OFFICE: 1991-500-063/22071

Standard Form 298 (Rev. 2-89)
Prescribed by ANSI Std. Z39-18
298-102